Theoretical Study on Mechanisms and Kinetics of NCCO + O_2 Reaction

Yizhen Tang,[†] Rongshun Wang,*[,†] and Baoshan Wang*[,‡]

Institute of Functional Material Chemistry, Faculty of Chemistry, Northeast Normal University, Renmin Road 5268, Changchun, Jilin 130024, P. R. China, and College of Chemistry and Molecular Sciences, Wuhan University, Wuhan 430072, P. R. China

Received: January 15, 2008; Revised Manuscript Received: March 18, 2008

Mechanisms and kinetics of the NCCO + O_2 reaction have been investigated using the extrapolated full coupled cluster theory with the complete basis set limit (FCC/CBS) and multichannel RRKM theory. Energetically, the most favorable reaction route involves the barrierless addition of the oxygen atom to one of the carbon atoms of NCCO and the subsequent isomerization−decomposition via the four-center intermediate and transition state, leading to the final products NCO and CO_2. At 298 K, the calculated overall rate constant is strongly pressure-dependent, which is in good agreement with the available experimental values. It is predicted that the high-pressure limit rate constants exhibit negative temperature dependence below 350 K. The dominant products are NCO and CO_2 at low pressures (ca. <10 Torr) and the NCCO(O_2) radical at higher pressures, respectively.

I. Introduction

Nitrogen−oxygen−carbon chain molecules, NC_nO, play important roles in interstellar space and in astrophysical chemistry.[1–4] The NCCO radical has attracted considerable experimental and theoretical attentions.[5–10] It has been established that the NCCO radical is the major gaseous product of the photodissociation of carbonylcyanide ($CO(CN)_2$). Moreover, NCCO is one of the important intermediates in combustion and in the nitric oxide reburning processes.[2,4] It is desirable to study the oxidation reaction of NCCO to understand the lifetime and evolution of this radical species in both atmosphere and combustion.

Experimentally, the NCCO + O_2 reaction has been investigated by Imamura and co-workers.[10] The NCCO radical was generated by the photodissociation of acetylcyanide. The rate constants were measured by monitoring the temporal decay of the radical concentrations. At 298 K, the rate constants were shown to be pressure dependent in the range 2.0−15.5 Torr of N_2. For example, $k = 5.4 \times 10^{-13}$ cm^3 molecule^{-1} s^{-1} at 2.0 Torr and k increases to 8.8×10^{-13} cm^3 molecule^{-1} s^{-1} at 15.5 Torr.

In this work, the mechanism of the NCCO + O_2 reaction is investigated using the high-level ab initio molecular orbital methods. Moreover, the rate constants are calculated using the multichannel RRKM theory over a wide range of temperatures and pressures.

II. Computational Methods

Geometries of the reactants, products, intermediates, and transition states for the NCCO + O_2 reaction were optimized using the density functional theory (DFT-B3LYP) with the standard 6-311G(d) basis set. Harmonic vibrational frequencies and the zero-point energies (ZPE) were calculated at the same level of theory. Minimum is characterized by its all real frequencies. The transition state has only one imaginary frequency. Intrinsic reaction coordinate (IRC) calculations were carried out at the B3LYP/6-311G(d) level to confirm the connection of the transition state with the designated reactants and products. Although the structural parameters of the species involved in the NCCO + O_2 reaction are considered to be reasonable with the density functional theory, the energetics of the species, especially the transition states, should be calculated at the higher level of theory because the reaction kinetics depend strongly on the barrier heights and the heats of reaction. Therefore, the single-point energy calculations have been carried out using the coupled cluster theory with the single and double excitations (CCSD) and augmented by a perturbative correction for connected triple excitations [CCSD(T)]. To avoid the problem of the spin contamination, a spin restricted scheme for the CCSD(T), namely, RCCSD(T), was used with the spin restricted open-shell Hartree−Fock (ROHF) reference. The RCCSD(T) energies were calculated with the correlation-consistent basis sets, i.e., cc-pVDZ and cc-pVTZ, and then were extrapolated to the complete basis set (CBS) limit values according to the expression of Helgaker and co-workers (abr. CBS1):[11]

$$E_X = E_\infty + aX^{-3} \tag{1}$$

and to the expression of Truhlar (abr. CBS2):[12] $E_{HF,\,X} = E_{HF,\,\infty} + bX^{-\alpha}$

$$E_{\mathrm{HF},X} = E_{\mathrm{HF},\infty} + bX^{-\alpha} \qquad E_{\mathrm{corr},X} = E_{\mathrm{corr},\infty} + cX^{-\beta} \tag{2}$$

where E_X, $E_{\mathrm{HF},X}$ and $E_{\mathrm{corr},X}$ are the RCCSD(T), ROHF, and correlation energies as a function of the cardinal number X of the cc-pVXZ basis sets, and $\alpha = 3.4$ and $\beta = 2.4$, respectively. It is known that the pertubational energy of the connected triple excitations accounts for only 75−80% of the full triple- and higher-order contributions. Therefore, the full coupled-cluster/complete basis set (FCC/CBS) energy was obtained by adding the CI truncation error correction ($E^{\mathrm{T}}_{\mathrm{CCSD(T)/cc\text{-}pVTZ}}/5$). The ab initio calculations were carried out using the Gaussian03[13] and Molpro[14] programs.

* Corresponding authors. E-mail address: R.W., wangrs@nenu.edu.cn; B.W., baoshan@whu.edu.cn. Tel: +86-431-85099511. Fax: +86-431-85099511

[†] Northeast Normal University.

[‡] Wuhan University.

10.1021/jp800394h CCC: $40.75
Published on Web 05/14/2008

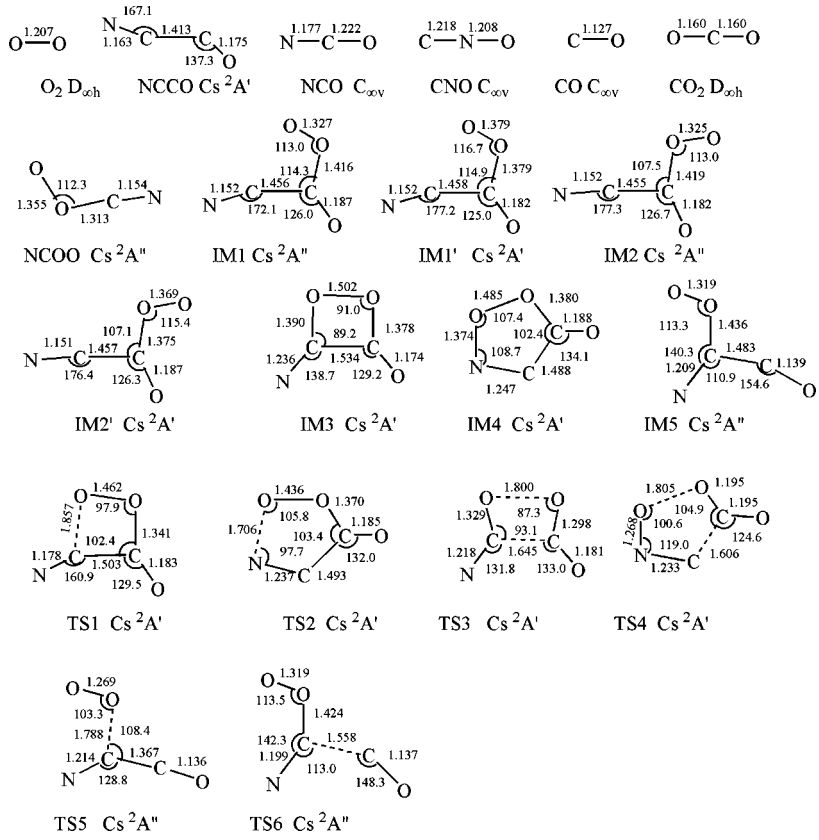

Figure 1. Geometries of the various species of the NCCO + O_2 reaction optimized at the B3LYP/6-311G(d) level. Bond distances are in angstrom and bond angles are in degrees.

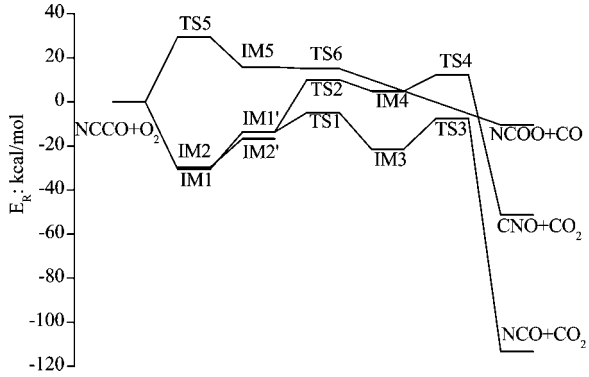

Figure 2. Energetic reaction routes of the NCCO + O_2 reaction. The energies correspond to the data calculated at the FCC/CBS2 level of theory.

III. Results and Discussion

The optimized geometries of the stationary points at the B3LYP/6-311G(d) level of theory are shown in Figure 1. The energetic reaction routes calculated at the FCC/CBS2 level are shown in Figure 2. The relative energies obtained at the B3LYP/6-311G(d), RCCSD(T)/cc-pVDZ, RCCSD(T)/cc-pVTZ, FCC/CBS1, and FCC/CBS2 levels of theory and the B3LYP/6-311G(d) calculated ZPE corrections are listed in Table 1.

It is noted that the spin contamination for the open-shell species involved in the NCCO + O_2 reaction has been overcome by using the spin-restricted method in this work. To assess the multiconfigurational characteristics of the reaction paths, the T_1 diagnostic values of the RCCSD(T) wave functions are monitored (see Table 1). Evidently, the T_1 diagnostic values of all the species are less than 0.04, which implies a negligible multireference character of the wave functions. However, TS3 is an exception, of which the value of T_1 diagnostic is as high as 0.062, indicating of the severe multiconfiugration characteristic. As a result, the calculated energetic of TS3 might be less reliable than the other data. Fortunately, the energy of TS3 appears to be significantly lower than that of the initial reactants. Therefore, the uncertainty in the barrier height for TS3 might not affect the reaction mechanism and the rate constants considerably.

As shown in Table 1, the two extrapolation procedures for the FCC/CBS energies give nearly the same data. The Truhlar's CBS2 energies tend to be slightly lower than the Helgaker's CBS1 data. Because only the double- and triple-ξ basis sets were employed in the extrapolation, the CBS2 energetics is preferable and they are used in the following discussion unless otherwise stated.

1. Reaction Mechanisms. As indicated by the atomic spin of the $NC_\alpha C_\beta O$ radical, the unpaired electron is delocalized along the NCCO skeleton. However, the β-C atom still has the largest spin density, i.e., 0.568, indicating that the reaction prefers to take place involving this radical center. The O_2 molecule approaches the C_β atom of the $NC_\alpha C_\beta O$ radical to form the intermediate NCC(O)O_2 radical, denoted as IM1 (*trans* conformer) or IM2 (*cis* conformer) depending on the dihedral angle of OOCO. Because the ground-state O_2 is in $X^3\Sigma_g^-$ and NCCO is in $^2A'$, both IM1 and IM2 have C_s symmetry and $^2A''$ electronic ground states. The association path is exothermic by about 30 kcal/mol. No transition state was found for the association at the B3LYP/6-311(d) level of theory.

Two subsequent reaction pathways were examined in view of the geometry of IM1. The first path takes place via a four-member-ring transition state, TS1, as shown in Figure 1. The terminal oxygen atom is bent to the C_α atom, forming a cyclic OOCC structure. The second path occurs via a five-member-

TABLE 1: ZPE Corrections, T_1 Diagnostic, and Relative Energies (in kcal/mol) at Various Levels of Various Species Involved in the NCCO + O_2 Reaction

species	ZPE	T_1 diagnostic	B3LYP	pVDZ[a]	pVTZ[b]	CBS1	CBS2
NCCO + O_2	11.0	0.018	0.0	0.0	0.0	0.0	0.0
NCO + CO_2	13.6	0.025	−112.6	−112.1	−115.1	−113.5	−113.4
CNO + CO_2	12.9	0.026	−50.2	−50.0	−52.3	−51.4	−51.4
NCOO + CO	11.3	0.026	−4.0	−9.1	−10.7	−10.7	−10.5
IM1	14.3	0.025	−23.2	−27.2	−31.6	−30.1	−30.6
IM1′	14.1	0.021	−7.0	−10.2	−14.6	−13.3	−13.8
IM2	14.4	0.025	−22.9	−27.0	−31.0	−29.3	−29.8
IM2′	14.3	0.021	−10.0	−13.7	−17.9	−16.2	−16.7
IM3	14.7	0.022	−11.1	−14.8	−21.6	−21.1	−21.5
IM4	14.8	0.025	15.3	12.1	5.2	5.3	4.9
IM5	12.8	0.034	20.1	20.8	17.0	16.4	15.9
TS1	13.1	0.030	1.9	2.1	−3.4	−4.2	−4.8
TS2	13.7	0.031	19.2	12.1	11.7	10.5	10.4
TS3	12.6	0.062	−2.2	−0.5	−4.0	−6.9	−7.5
TS4	13.4	0.033	19.0	18.3	14.2	12.8	12.4
TS5	12.4	0.039	29.3	36.7	32.1	30.1	29.5
TS6	12.4	0.033	19.7	19.6	16.4	15.5	15.1

[a] pVDZ: energies at the RCCSD(T)/cc-pVDZ level. [b] pVTZ: energies at the RCCSD(T)/cc-pVTZ level.

ring transition state, TS2, in which the terminal oxygen atom is attached to the terminal N atom, forming a cyclic OOCCN structure. It is interesting to note that the barrier for TS1 is significantly lower than that for TS2. With respect to the initial NCCO + O_2 regents, the energy of TS1 is about −5 kcal/mol and that of TS2 is about +10 kcal/mol. On the other hand, it is worth noting that both TS1 and TS2 have C_s symmetry and the $^2A'$ electronic states. Obviously, they cannot connect with the ground-state IM1 intermediate because of the symmetry forbidden. The IRC calculation showed that TS1 and TS2 correlate with the electronically excited NCC(O)O_2 radical of $^2A'$ state, IM1′, as shown in Figure 1. For both IM1($^2A''$) and IM1′($^2A'$), the unpaired electron is mainly located at the terminal oxygen atom, which possesses one pair of lone electrons as well. The electron configuration of IM1′ is different from that of IM1 by the orientation of the singly occupied p orbital of the terminal oxygen atom, i.e., in-plane for IM1′ and out-of-plane for IM1, respectively. Consequently, the stronger repulsion between the two lone-pair electrons on the two oxygen atoms exists in IM1′ than that in IM1. Moreover, the unpaired electron in IM1 is delocalized somehow between the two oxygen atoms. Therefore, IM1′ is considerably less stable than IM1. The energy of IM1′ is about 17 kcal/mol higher than that of IM1.

The lower barrier height for TS1 than that for TS2 can be understood through the analysis of the structural feature and the charge distributions. TS1 is an early barrier but TS2 is a late barrier. As shown in Figure 1, the forming OC_α bond of TS1 is as long as 1.86 Å, which is 0.47 Å longer than the equilibrium distance in the product. In TS2, the forming ON bond is 1.71 Å, which is 0.34 Å longer than the equilibrium distance in the product. The structural feature is in accordance with the spin density distributions of TS1 and TS2. For TS1, the spin densities on the terminal O and the terminal N atoms change from 0.90 to 0.64 and from 0 to 0.50, respectively. As for TS2, the spin densities on the terminal O and the C_α atoms change from 0.90 to 0.48 and from 0 to 0.70, respectively. In view of the charges of the NCC(O)O_2 ($^2A'$) radical, the negatively charged terminal O atom (−0.01e) certainly prefers to react with the positively charged C_α atom (0.03e) instead of the negatively charged N atom (−0.17e).

As mentioned above, IM1′ in the electronically excited $^2A'$ state does not correlate to the NCCO ($^2A'$) + O_2 ($X^3\Sigma_g^-$) reactants. Therefore, after the formation of the nonreactive ground $^2A''$ state of the NCC(O)O_2 radical, the reaction breaks C_s symmetry by rotating the terminal oxygen atom to align its p orbitals, and then surmounts the barriers TS1 and TS2, forming the intermediates IM3 and IM4, respectively. The formation of IM3 is exothermic by about 22 kcal/mol, and the formation of IM4 is endothermic by about 5 kcal/mol. Therefore, IM4 is less stable than IM3, although IM4 shows a five-member-ring cyclic geometry.

The decomposition of IM3 produces NCO radical and CO_2 molecule through a concerted OO and CC bond cleavages. The corresponding transition state is TS3. As shown in Figure 1, the CC bond is only slightly stretched by about 7%, whereas the OO bond is elongated by about 20%. The energy of TS3 is 7.5 kcal/mol lower than that of the NCCO + O_2 regent. As mentioned above, TS3 is subject to severe mulitconfigurational character. The barrier for TS3 might be only qualitatively reliable. The NCO + CO_2 channel is highly exothermic by 113.4 kcal/mol. It is conceivable that the major products are NCO and CO_2 in the oxidation of the NCCO radicals.

As for IM4, a similar CO_2-elimination channel exists. The transition state is TS4, as shown in Figure 1. The CC and OO bonds are breaking simultaneously, leading to CNO and CO_2. This channel is less exothermic than the NCO + CO_2 channel because the CNO radical is less stable than NCO. Moreover, the barrier for TS4 is as high as 12.4 kcal/mol. Therefore, the CNO + CO_2 channel cannot be significant.

The addition of oxygen to the α-C atom of the $NC_\alpha C_\beta O$ radical has also been investigated. As expected, a significant barrier, namely, TS5 (with C_s symmetry and in $^2A''$ state), is involved in the addition pathway. The barrier height is nearly 30 kcal/mol. Moreover, the addition is endothermic. The adduct is shown as IM5 in Figure 1. However, IM5 is a very unstable radical. Not only is its energy 15.9 kcal/mol higher than that of the reagents but also it decomposes rapidly through stretching the CC bond slightly via TS6 to form NCOO and CO. Evidently, the CO production channel is negligible in the NCCO + O_2 reaction.

In summary, the predominant mechanism for the NCCO + O_2 reaction includes the barrierless addition of O_2 to the carbonyl carbon atom of NCCO, forming the NCC(O)O_2 radical on the $^2A''$, surface. Subsequently, the reaction occurs on the $^2A'$ surface, generating NCO radicals and CO_2 molecules via a four-center route. The production of either CNO or CO is negligible.

2. Kinetics. For simplicity, the following scheme was employed in the kinetic simulation of the NCCO + O_2 reaction:

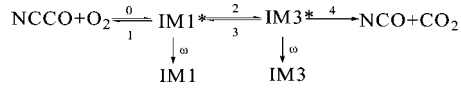

where "*" represents the vibrational excitation of the intermediates. The steady-state assumption was applied for all the excited intermediates and the multichannel RRKM theory was used to calculate the microcannonical rate constant for each reaction path.

$$k_{\mathrm{NCO+CO_2}}(T,P) = \frac{l_a}{h}\frac{Q_t^{\neq}Q_r^{\neq}}{Q_{\mathrm{NCCO}}Q_{\mathrm{O_2}}}e^{-E_a/RT}\int_0^{\infty}\frac{k_4X_3}{X_4}N_0(E^{\neq})e^{-E^{\neq}/RT}\,dE^{\neq}$$

$$k_{\mathrm{IM1}}(T,P) = \frac{l_a}{h}\frac{Q_t^{\neq}Q_r^{\neq}}{Q_{\mathrm{NCCO}}Q_{\mathrm{O_2}}}e^{-E_a/RT}\int_0^{\infty}\frac{\omega}{X_4}N_0(E^{\neq})e^{-E^{\neq}/RT}\,dE^{\neq}$$

$$X_1 = k_1 + k_2 + \omega$$

$$X_2 = k_3 + k_4 + \omega$$

$$X_3 = k_2/X_2$$

$$X_4 = X_1 - k_3X_3$$

$$k_i(E) = \alpha_i k_i\sqrt{\frac{I_i^{\neq}}{I_j^{IM}}}\frac{N(E-E_i^{\neq})}{h\rho_j(E)} \qquad i=1,2;\ j=1,2$$

where Q_{NCCO} and $Q_{\mathrm{O_2}}$ are the total partition functions of NCCO and O_2, respectively. l_a is the statistical factor (degeneracy) for the association step a; E_a, $Q_t^{\pm}$, $Q_r^{\pm}$, and $N_0(E^{\pm})$ are the corresponding barrier height, the translational and rotational partition functions, and the number of states. α_i is the statistical factor for the ith reaction path degeneracy; κ_i is the tunneling factor; $I_i^{\pm}$andI_j^{IM} are the moments of inertia ($I_aI_bI_c$) of the transition state i and the intermediate j; h is Planck's constant; $\rho_j(E)$ is the density of states at energy E of the intermediate j; $N(E - E_i^{\pm})$ is the number of states of the transition state i at the energy above the barrier height for transition state i. The density of states and the number of states are calculated using the extended Beyer−Swinehart algorithm.[15,16] The collision deactivation rate $\omega = \beta_c Z_{\mathrm{LJ}}[\mathrm{M}]$, where β_c is the collision efficiency calculated using Troe's weak collision approximation with the energy transfer parameter $-\langle\Delta E\rangle$. Z_{LJ} is the Lennard-Jones collision frequency. [M] is the pressure of the bath gas (N_2 in this work). It is noted that the overall rate constants correspond to the sum of the above two rate constants.

Because the association between NCCO and O_2 is barrierless, the energetic profile along the reaction coordinate has to be treated variationally. The relative energies were calculated at the B3LYP/6-311G(d) level of theory by fixing the reacting C···O bond from 2 to 4 Å with a step size of 0.1 Å and then were scaled to the FCC/CBS2 level by a factor of 1.32 ($D_e^{\mathrm{FCC}}/D_e^{\mathrm{B3LYP}}$, e.g., the ratio of the binding energies of IM1 calculated at either FCC/CBS2 or B3LYP/6-311G(d) levels of theory). The energy and the rotational constant for each point were obtained by interpolation. The vibrational frequencies were considered to be those of the reactants (NCCO and O_2), together with the four "intermolecular modes" after excluding the C···O stretch vibration along the reaction coordinate. Among the four "disappearing" frequencies, the O−O bond rotation around the CO axis has been considered to be a one-dimension free internal rotor with the reduced moment of inertia of 47.5 amu. The other three disappearing vibrational frequencies were calculated from the corresponding normal modes of IM1 using the following exponential expression: $\nu(R_e) \times e^{-\alpha\ (R-R_e)}$, where R_e is the equilibrium distance of the CO bond in IM1. The scaling parameter α is set to be 1.1 empirically.

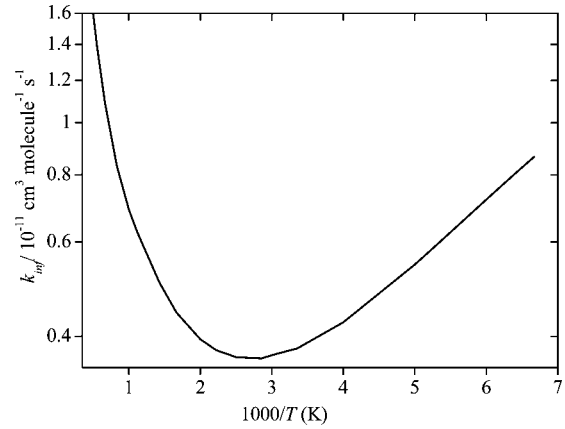

Figure 3. High-pressure limit rate constants (k_{inf}) for the NCCO + O_2 reaction in the temperature range 150−2000 K.

The high-pressure limit rate constants for the title reaction are shown in Figure 3. Apparently, the rate constants exhibit negative temperature dependence below 350 K. For example, as the temperature drops from 298 to 150 K, the rate constant increases by almost twice. Certainly, such a prediction is subject to significant uncertainty because the high-pressure limit rate constants are very sensitive to the treatment of the entrance barrier. More precisely, in the current model, the values of the internal rotational constant and the scaling factor for the disappearing frequencies along the entrance pathway can affect the high-pressure limit kinetics significantly, even if the energies of the minimum energy path (MEP) can be calculated accurately. Before the experimental data for the high-pressure limit kinetics are available, the theoretical modeling gives an insight to the kinetic character of the NCCO + O_2 reaction at low temperatures of atmospheric interest. For convenience, an empirical three-parameter expression, namely,

$$k_{\mathrm{inf}}(T)\ (\mathrm{cm^3\ molecule^{-1}\ s^{-1}}) = 4.53\times 10^{-17}T^{1.64}\exp(-593/T),$$

was employed to represent the rate constant over the temperature range 150−2000 K.

The pressure-dependent rate constants were calculated at 298 K. The pressure of N_2 bath gas ranges from 10^{-2} to 10^6 Torr. The calculated rate constants as well as the available experimental values are shown in Figure 4. The weak-collision approximation was used to estimate the energy transfer rate. The interaction energies between IM1 and N_2 have been calculated at the MP2/6-31+G(d) level, and the Lennard-Jones 12-6 potential was used to fit the interaction energies to obtain the potential well (ϵ = 1841 K) and the collisional diameter (σ = 2.65 Å). The energy transfer parameter, $-\langle\Delta E\rangle$, i.e., the average energy transferred per collision, was calculated to be around 1000 $\mathrm{cm^{-1}}$ by fitting the experimental rate constants in the range 2.0−15.5 Torr. Usually N_2 is an efficient quencher for the radical intermediates. This is in agreement with the fact that there is a strong interaction between IM and N_2, as calculated at 1800 K (e.g., ∼15 kJ/mol). As a matter of fact, it

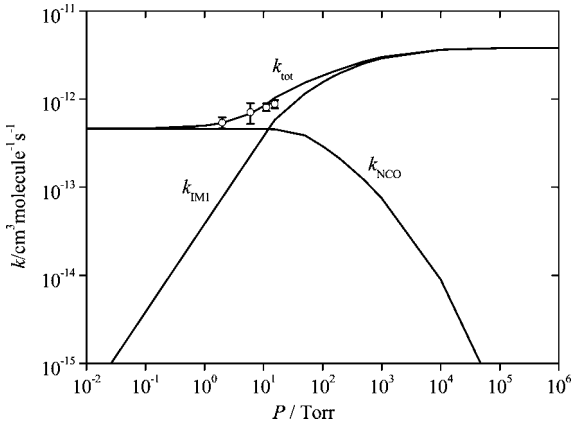

Figure 4. Pressure dependent rate constants for the NCO + CO_2 channel, k_{NCO}, for the deactivation of the initial adduct IM1, k_{IM1}, and the overall rate constant, k_{tot}, for the NCCO + O_2 reaction in the range $10^{-2}-10^6$ Torr of N_2 bath gas at 298 K. The experimental data are shown in open circles for comparison.

has been shown that the quenching efficiency of N_2 is much higher than the monatomic bath gases such as He. It is worth noting that the overall rate constant is independent of the value of $-\langle\Delta E\rangle$ although the branching ratios of the products are sensitive to the value of $-\langle\Delta E\rangle$.

As seen from Figure 4, the calculated overall rate constants show typical "S" falloff behavior and strong pressure dependence in the range $1-10^5$ Torr, which are in good agreement with the experimental data. Only two individual rate constants, namely, k_{NCO} for the NCO + CO_2 channel and k_{IM1} for the deactivation of the IM1, are of significance. As the pressure increases, k_{NCO} decreases whereas k_{IM1} increases. In the falloff region, the two reaction channels compete effectively. The yield of IM1 is nearly 100% at pressures higher than 500 Torr. This indicates that the NCCO + O_2 reaction at atmosphere will produce the IM1 radical dominantly, which may initialize other radical reactions subsequently. At lower pressures, for example, below 1 Torr, the yield of NCO and CO_2 is close to 100%. Therefore, the production of CO_2 and NCO radical dominates the oxidation of the NCCO radical. Because the NCO + CO_2 channel is the most exothermic channel in the NCCO + O_2 reaction, it is conceivable that the low-pressure oxidation of NCCO radical, especially under the atmospheric condition, leads to the CO_2 molecules. The NCO radicals may continue to react with O_2, forming CO, CO_2, NO, or NO_2.

Under the typical atmospheric condition ($T = 250$ K and $P = 5$ Torr), the individual rate constants are 5.93×10^{-13} and 3.55×10^{-13} cm^3 molecule^{-1} s^{-1} for the NCO + CO_2 channel and the IM1 deactivation, respectively. The major products are NCO + CO_2 with the yield of 63% and IM1 is the minor product with the yield of 37%. Correspondingly, under the typical combustion condition ($T = 2500$ K and $P = 760$ Torr), the individual rate constants are 1.25×10^{-13} and 8.46×10^{-16} cm^3 molecule^{-1} s^{-1}, respectively. Evidently, the NCO + CO_2 channel is dominant and the deactivation of IM1 is negligible.

IV. Conclusions

Using the full coupled-cluster theory with the complete basis set limit extrapolation, we have calculated the energetically accessible reaction routes for the NCCO + O_2 reaction. Both the reaction mechanism and the kinetic characteristics have been revealed on the basis of the sound ab initio data. It is confirmed that the most favorable reaction mechanism takes place via the oxygen atom attacking on the carbonyl C atom of the NCCO radical to form the NCCO(O_2) radical adduct (IM1). Subsequently, IM1 isomerizes to another four-member-ring structure (IM3), which decomposes by the concerted CC and OO bond cleavages to form the final products NCO and CO_2. The rate constants of the NCCO + O_2 reaction show strong temperature and pressure dependence. At temperatures below 350 K, the high-pressure limit rate constants might be negatively temperature dependent. At room temperature (298 K), the falloff behavior exists in the range $1-10^5$ Torr of N_2. As a result, the major nascent products of the NCCO oxidation can be the IM1 radical intermediate ($p > 10$ Torr) or NCO + CO_2 ($p < 10$ Torr).

Acknowledgment. This work was supported by the National Science Foundation of China No. 20773021 and No. 20673079.

References and Notes

(1) Williams, B. A.; Pasternack, L. *Combust. Flame* **1997**, *111*, 87.
(2) Kruse, T.; Roth, P. *Int. J. Chem. Kinet.* **1999**, *31*, 11.
(3) Becker, K. H.; Schmidt, F.; Wiesen, P. *Phys. Chem. Chem. Phys.* **2000**, *214*, 503.
(4) Ristanovic, A.; Fernandez, A.; Fontijn, A. *J. Phys. Chem. A* **2002**, *106*, 8291.
(5) Furlan, A.; Scheld, H. A.; Huber, J. R. *Chem. Phys. Lett.* **1998**, *282*, 1.
(6) Sumiyoshi, Y.; Takada, H.; Endo, Y. *Chem. Phys. Lett.* **2004**, *387*, 116.
(7) Francisco, J. S.; Liu, R. F. *J. Chem. Phys.* **1997**, *107*, 3840.
(8) Yu, G. T.; Ding, Y. H.; Huang, X. R.; Sun, C. C. *J. Phys. Chem. A* **2005**, *109*, 2364.
(9) Jursic, B. S. *J. Mol. Struct. (THEOCHEM).* **1999**, *460*, 207.
(10) Imamura, T.; Washida, N. *Int. J. Chem. Kinet.* **2000**, *11*, 440.
(11) Halkier, A.; Helgaker, T.; Jorgensen, P.; Klopper, W.; Koch, H.; Olsen, J.; Wilson, A. K. *Chem. Phys. Lett.* **1998**, *286*, 243.
(12) Truhlar, D. G. *Chem. Phys. Lett.* **1998**, *294*, 45.
(13) Frisch, M. J.; Truck, G. W.; Schlegel, H. B.; Scuseria, G. E.; Robb, M. A.; Cheeseman, J. R.; Zakrzewski, V. G.; Montgomery, J. A., Jr.; Stratmann, R. E.; Burant, J. C.; Dapprich, S.; Millam, J. M.; Daniels, A. D.; Kudin, K. N.; Strain, M. C.; Farkas, O.; Tomasi, J.; Barone, V.; Cossi, M.; Cammi, R.; Mennucci, B.; Pomelli, C.; Adamo, C.; Clifford, S.; Ochterski, J.; Petersson, G. A.; Ayala, P. Y.; Cui, Q.; Morokuma, K.; Malick, D. K.; Rabuck, A. D.; Raghavachari, K.; Foresman, J. B.; Cioslowski, J.; Ortiz, J. V.; Boboul, A. G.; Stefnov, B. B.; Liu, G.; Liaschenko, A.; Piskorz, P.; Komaromi, L.; Gomperts, R.; Martin, R. L.; Fox, D. J.; Keith, T.; Al-Laham, M. A.; Peng, C. Y.; Nanayakkara, A.; Gonzalez, C.; Challacombe, M.; Gill, P. M. W.; Johnson, B.; Chen, W.; Wong, M. W.; Andres, J. L.; Gonzalez, C.; Head-Gordon, M.; Replogle, E. S.; Pople, J. A. *GAUSSIAN 03*, revision D.01; Guassian, Inc.: Pittsburgh, PA, 2003.
(14) Werner, H. J.; Knowles, P. J.; Lindh, R.; Manby, F. R.; Schutz, M.; et al. See http://www.molpro.net. *MOLPRO*, version 2006.1, a package of ab initio programs.
(15) Stein, S. E.; Rabinovitch, B. S. *J. Chem. Phys.* **1973**, *58*, 2438.
(16) Astholz, D. C.; Troe, J.; Wieters, W. *J. Chem. Phys.* **1979**, *70*, 5107.

JP800394H